

# An Inorganic Biopolymer Polyphosphate Controls Positively Charged Protein Phase Transitions

Xin Wang, Chenke Shi, Jianbin Mo, Yun Xu, Wei Wei,\* and Jing Zhao\*

Dedicated to the 100th anniversary of the School of Chemistry and Chemical Engineering, Nanjing University

**Abstract:** Polyphosphate (PolyP) is one of the most compact inorganic polyanionic biopolymers that participates in various physiological processes. However, the mechanism of the interaction between polyP and proteins remains poorly understood. Herein, we report that polyP can interact with positively charged green fluorescent protein, +36GFP, resulting in liquid–liquid phase separation (LLPS) by intermolecular electrostatic interactions in cells. Upon nutrient deprivation, genetically engineered *Citrobacter freundii* accumulates intracellular polyP at a rate of  $210 \mu\text{M min}^{-1}$ , resulting in the compartmentation of +36GFP at the cell poles within 1 h. Medium chain-length polyP (60-mer) could induce the formation of +36GFP coacervates in vitro at a protein concentration as low as 200 nM, which is of the same magnitude as native proteins. In contrast, shorter polyP (14-mer) could not induce LLPS under the same conditions. This may offer a general approach to manipulate protein–protein interactions through LLPS.

Inorganic polyphosphate (polyP) was first revealed by Kornberg et al. to play key roles in the stress resistance, colonization, and infection of microorganisms.<sup>[1]</sup> PolyP is one of the most compact polyanionic biopolymers due to its structural simplicity. It emerged during prebiotic times and is conserved from bacteria to *Homo sapiens*.<sup>[2]</sup> Compared with organic polyanionic biomolecules (nucleic acids), inorganic polyP possesses the following distinct features: 1) no genetic information involvement because of the lack of sequence differences; and 2) no higher structure arising from the monotonic repeat of phosphates. Later, work from other groups demonstrated that polyP is implicated in blood

clotting, bone mineralization, and apoptosis in eukaryotes.<sup>[3]</sup> This series of seemingly unrelated functions poses an intriguing question as to how a simple polyanion, such as polyP, can fulfill these various roles. Early work by Kornberg et al. showed that polyP could stimulate Lon-protease-mediated degradation of ribosomal proteins.<sup>[1a]</sup> Pioneering studies from Jakob et al. suggested that polyP might serve as a polyanionic scaffold for protein functioning.<sup>[4]</sup> The significant breakthrough made by Goto et al. demonstrated that polyP could act with  $\beta_2$ -microglobulin, either through electrostatic attraction at acidic pH or via Hofmeister effects at neutral pH, to exert effects in the progression of dialysis-related amyloidosis.<sup>[5]</sup> Therefore, the interplay of polyP with proteins may be one of the unifying principles through which polyP achieves diverse physiological functions.

Pivotal progress was made by Alberti, Chen, and Hyman who showed that eukaryotes spatially and temporally organize their cytoplasm and nucleoplasm via liquid–liquid phase separation (LLPS), the supramolecular assemblies of proteins, DNA, and RNA.<sup>[6]</sup> The driving forces of LLPS include multivalent macromolecular interactions, proteins with modular domains, proteins with intrinsically disordered regions, and patterned intermolecular electrostatic interactions between acidic and basic tracts.<sup>[7]</sup> Thus, we set out to explore whether polyP, as the most compact intracellular polyanion, can control the phase behavior of proteins through electrostatic interactions. In this study, we induced the assembly of positively charged green fluorescent protein (+36GFP) into liquid-like droplets in *Citrobacter freundii* engineered to accumulate polyP. A routinely used cationic dye, DAPI, can thoroughly abolish the occurrence of this process, indicating that electrostatic effects are the major driving force. Subsequent in vitro results showed that polyP does indeed drive +36GFP-droplet formation under physiological conditions. These results indicate that inorganic polyanionic polyphosphate can be used to manipulate protein–protein interactions through LLPS (Scheme 1).

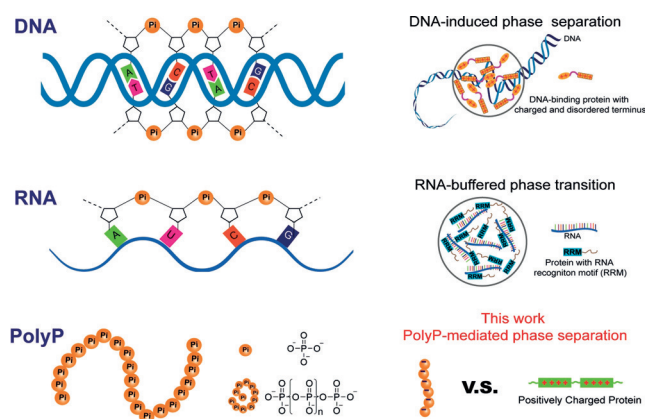
In our previous work, we obtained a *C. freundii* derivative (CPP) that overexpressed the native polyphosphate kinase (PPK1) from a medium-copy plasmid.<sup>[8]</sup> CPP did not accumulate any detectable polyP when cultured in nutrient-rich LB broth but initiated marked intracellular polyP synthesis upon transfer to a nutrient-poor synthetic wastewater medium (SMW). Using CPP as the initial strain, a compatible tightly regulated pBAD33 plasmid that harbored the gene encoding positively charged green fluorescent protein (+36GFP, each GFP possesses a net positive charge of 36) was introduced to obtain a new *C. freundii* derivative,

[\*] Dr. X. Wang, J. Mo, Prof. Dr. W. Wei, Prof. Dr. J. Zhao  
State Key Laboratory of Coordination Chemistry,  
Chemistry and Biomedicine Innovation Center (ChemBIC),  
School of Chemistry and Chemical Engineering, Nanjing University  
Nanjing 210093 (P. R. China)  
E-mail: jingzhao@nju.edu.cn

Dr. X. Wang, C. Shi, Y. Xu, Prof. Dr. W. Wei  
State Key Laboratory of Pharmaceutical Biotechnology,  
School of Life Science, Nanjing University  
Nanjing 210093 (P. R. China)  
E-mail: weiwei@nju.edu.cn

Prof. Dr. W. Wei, Prof. Dr. J. Zhao  
Shenzhen Research Institute, Nanjing University  
Shenzhen, 518000 (P. R. China)

Supporting information and the ORCID identification number(s) for the author(s) of this article can be found under:  
<https://doi.org/10.1002/anie.201913833>.



**Scheme 1.** Summary diagram of protein phase separation reported to be induced or buffered by nucleic acids (organic polyanions). PolyP can mediate the phase separation of positively charged protein in this work.

designated CPG. By doing so, a certain amount of intracellular +36GFP could form during cultivation in LB broth, and its concentration remained unaltered after the removal of the LB broth and arabinose, the chemical inducer of +36GFP expression. Therefore, we could investigate the possible phase change of +36GFP in cells by changing the intracellular polyP concentration while keeping the +36GFP concentration constant. As shown in Figure 1A, when the CPG cells collected from the LB medium were transferred to SMW, the disperse +36GFP signal condensed to both polar ends of each CPG cell, a localization pattern that precisely matched what

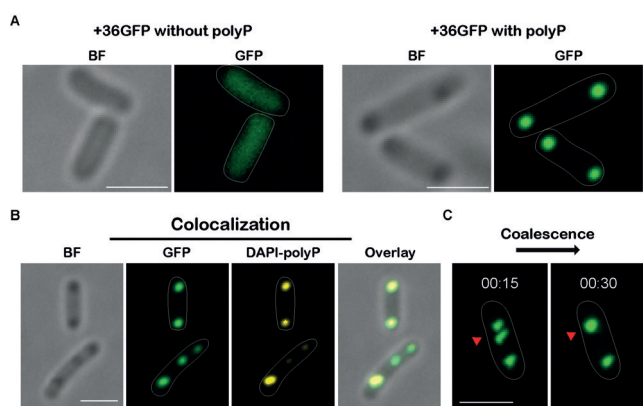


**Figure 1.** Intracellular polyP synthesis mediated +36GFP compartmentalization. A) Fluorescence microscopy images of CPG cells that were sampled from nutrient-rich LB broth (left panel) and nutrient-poor SMW (right panel). Scale bar, 2  $\mu\text{m}$ . B) Colocalization of intracellular fluorescent foci of the +36GFP and DAPI–polyP complexes. Images acquired from individual channels (bright field, GFP, and DAPI–polyP) are shown, and the overlay indicates colocalization. Scale bar, 2  $\mu\text{m}$ . The images shown in (A) and (B) are representative of at least ten fields examined. C) A typical fusion event (red arrowheads) indicative of the liquid-like property of the polyP/+36GFP complex. To reduce photobleaching effects, only two photographs were sequentially performed for one CPG cell with a time interval of 15 min. Scale bar, 2  $\mu\text{m}$ . The images are representative of at least three cells that were subjected to sequential imaging. All solid lines were manually added to the fluorescent images to indicate the bacterial outline. All the experiments were conducted independently at least three times.

we previously observed for polyP distribution in CPP.<sup>[8]</sup> This result implied that polyP might interact with +36GFP and guide the positioning of +36GFP via its own localization, thus achieving intracellular compartmentation. To support this hypothesis, we performed DAPI staining with CPG cells that harbored +36GFP granules. The overlapping of fluorescent foci emitted from +36GFP and DAPI–polyP complexes demonstrated their colocalization, which indicated that the compartmentation of +36GFP might be provoked by polyP synthesis (Figure 1B). During the imaging process, we observed a fusion event between two +36GFP plaques (Figure 1C), which raised the intriguing possibility that these polyP/+36GFP complexes might possess liquid-like properties.

To test this idea, we set out to capture a series of images of a single CPG cell to examine how this compartmentation progresses. A typical compartmentation process is shown in Figure 2A, which shows the intracellular +36GFP signal transforming from homo- to heterogeneous, and ultimately being sequestered at the polar regions within one cell. During this process, we observed that highly heterogeneous +36GFP plaques collide and coalesce, which is accompanied by enhanced fluorescence intensities, even though they were subject to significant photobleaching due to continuous imaging that therefore resulted in a rough edge instead of a spherical edge. Gel analysis of CPG cells sampled at the corresponding compartmentalizing stage showed that polyP synthesis was a concurrent event, which further demonstrated that the compartmentation of +36GFP is indeed driven by polyP (Figure 2B). Considering their net charges, we interpreted that electrostatic attraction between +36GFP and polyP was the major driving force.<sup>[9]</sup> This interpretation is also supported by the DAPI staining performed at the beginning of this process, namely, transferring those CPG cells collected from LB medium to SMW containing 10  $\mu\text{M}$  DAPI. The addition of DAPI thoroughly abolished the occurrence of +36GFP heterogeneity because the cationic dye DAPI preferentially binds with polyP and counteracts its negative charge (Figure 2C), thus eliminating the electrostatic interaction between +36GFP and polyP. Next, to better understand the phase of these polyP/+36GFP complexes, we sought to investigate the biophysical features of the +36GFP condensates intracellularly. A previous study has shown that the nutrient-rich cultivation of bacteria with intracellular polyP, performed under nutrient-poor conditions, can redirect polyP metabolism from synthesis to degradation.<sup>[10]</sup> According to this principle, we performed a simple test by transferring CPG cells that harbored polyP/+36GFP granules back to nutrient-rich LB medium. This resulted in the shrinkage of the +36GFP compartments and their eventual dissolution into the cytoplasm (Figure 2D). This phenomenon encouraged us to argue that the polyP/+36GFP granules might be liquid-like droplets rather than solid protein membrane-bound polyP entities. Thus, polyP-mediated intracellular +36GFP compartmentation in CPG cells might possibly be polyP-driven LLPS of +36GFP.

To test whether the observed intracellular LLPS-like phenomenon could be reconstituted independent of the bacterial cytoplasmic environment, we performed *in vitro*

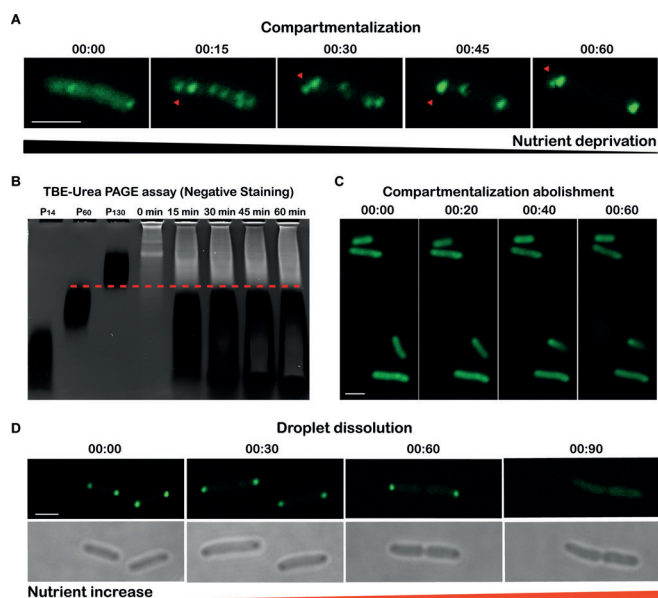


**Figure 2.** Assembly and disassembly of liquid-like +36GFP droplets in CPG cells. A) Nutrient-deprivation activated intracellular +36GFP compartmentalization, representing the formation and assembly progress of +36GFP condensates. The point in time at which CPG cells were transferred to SMW was set as 0 min, and a series of images of one CPG cell were captured at 15 min intervals. Colliding and coalescing of the fluorescent plaques are indicated by red arrowheads. Scale bar, 2  $\mu\text{m}$ . The images are representative of at least three independent experiments. B) TBE-Urea PAGE analysis of intracellular polyP formation in CPG cells during the compartmentalization progress. PolyP molecules of given chain lengths served as the markers. PolyP bands were visualized after negative staining; thus, dark regions represent polyP, while the bright regions in contrast to the gray background are DNA and RNA. The dashed line indicates the growth of polyP chains, approaching the top of the 60-mer band and bottom of the 130-mer band. C) Abolishment of +36GFP compartmentalization in CPG cells by the addition of DAPI. Imaging was performed at the same time interval as described in (A). Scale bar, 2  $\mu\text{m}$ . The compartmentalization-abolishing phenomenon existed in all cells examined. D) Nutrient increase induced the dissolution of +36GFP condensates. The point in time when CPG cells that harbored polarly localized +36GFP granules were transferred to LB (without arabinose) was set as 0 min. Imaging was performed with CPG cells sampled from LB thereafter at an interval of 30 min. Bright field images are given to show the bacteria outlines. Scale bar, 2  $\mu\text{m}$ . The images are representative of at least three independent experiments.

reactions with polyP and purified +36GFP under physiological salt conditions. First, intracellular +36GFP concentration and polyP content variation were measured to determine the critical parameters that might determine the phase transition of +36GFP. While +36GFP remained unaltered at 100 nM after the removal of the chemical inducer (i.e., arabinose), intracellular polyP continuously accumulated at a rate of 210  $\mu\text{M min}^{-1}$  (see the Supporting Information and Figure S1 in the Supporting Information for detailed analysis and calculation) after the CPG cells were transferred to SMW. Regarding the charge of the two molecules, we noticed that the net charge molar ratio ( $R-/+$ ) of polyP versus +36GFP remained greater than 1 throughout this process. This finding is quite similar to the droplet-generating situation that occurs between RNA (polyU, polyuridylic acid) and a positively

charged peptide.<sup>[11]</sup> Therefore, we speculated that the surplus of negative charge within the reaction system might be the prerequisite of the +36GFP phase transition. To test this hypothesis and to aid in visualization, 3.2 mM of commercially available heterogeneous polyP<sub>45</sub> was mixed with 5  $\mu\text{M}$  +36GFP to achieve an  $R-/+$  of approximately 17.7. The solution became turbid almost instantly, indicating the quick initiation of a phase change. The condensates formed possessed liquid properties, which was evidenced by either gravity-mediated coacervation in a 1.5 mL tube (Figure 3A, inset) or by the microscopic observation that spherical droplets formed on the glass bottom of Petri dishes (Figure 3A, right panel). Furthermore, a typical fusion event was also captured when the same components were mixed and immediately subjected to continuous imaging with a DeltaVision™ Ultra microscope (Figure 3B and Supporting Information, Movie S1). We next determined the phase distribution of polyP/+36GFP complexes by plotting the charge molar ratio  $R-/+$  against polyP<sub>45</sub> concentration. Although seemingly irregular, probably arising from the heterogeneity of polyP<sub>45</sub>, specific droplet formation regions could still be found in the diagram where polyP<sub>45</sub> caused +36GFP to undergo LLPS *ex vivo* (Figure 3C).

To test whether polyP molecules of different chain lengths might differ with respect to their abilities to mediate +36GFP phase separation, we determined the phase distributions of polyP molecules of different chain lengths (namely, polyP<sub>14</sub>, polyP<sub>60</sub>, and polyP<sub>130</sub>) with respect to +36GFP in the same concentration region as for polyP<sub>45</sub>. The results showed that both the 60-mer and 130-mer polyPs could induce the formation of +36GFP coacervate droplets when their concentrations exceeded 200  $\mu\text{M}$  (Figures 3D,E), whereas 14-mer polyP showed no ability to induce droplet formation even at an inorganic phosphate concentration as high as 3200  $\mu\text{M}$  (Supporting Information, Figure S2). When compared with heterogeneous polyP<sub>45</sub>, homogeneous polyPs (either 60-mer or 130-mer) mediated +36GFP phase distributions that were more regular and exhibited a clear concentration-dependent effect. Furthermore, for a given polyP concentration, as +36GFP concentration increased (corresponding to decreases in  $R-/+$ ; Figure 3D, right panel), the apparent volume of the dense phase increased significantly as indicated by the total droplet area in the corresponding image. This result is consistent with the phenomenon of the increased nucleic-acid-mediated droplet volume of an RNA-binding protein with a decrease in the RNA-to-protein molar ratio, which further demonstrates that the polyP-to-protein net charge molar ratio is a critical parameter and that a lower molar ratio may favor polyanion-induced protein coacervate droplets formation.<sup>[12]</sup> Remarkably, 200  $\mu\text{M}$  60-mer polyP was sufficient to induce the detectable formation of liquid droplets at +36GFP concentrations less than 200 nM, which is of the same magnitude as the concentration of +36GFP detected in CPG cells. This finding indicates that long-chain polyPs can shift the phase boundary of +36GFP to lower protein content, enabling their LLPS under physiological concentrations. Collectively, these results demonstrate that 1) polyP can indeed drive +36GFP to perform LLPS either in cells or *in vitro*; 2) the phase change promotion capacity of

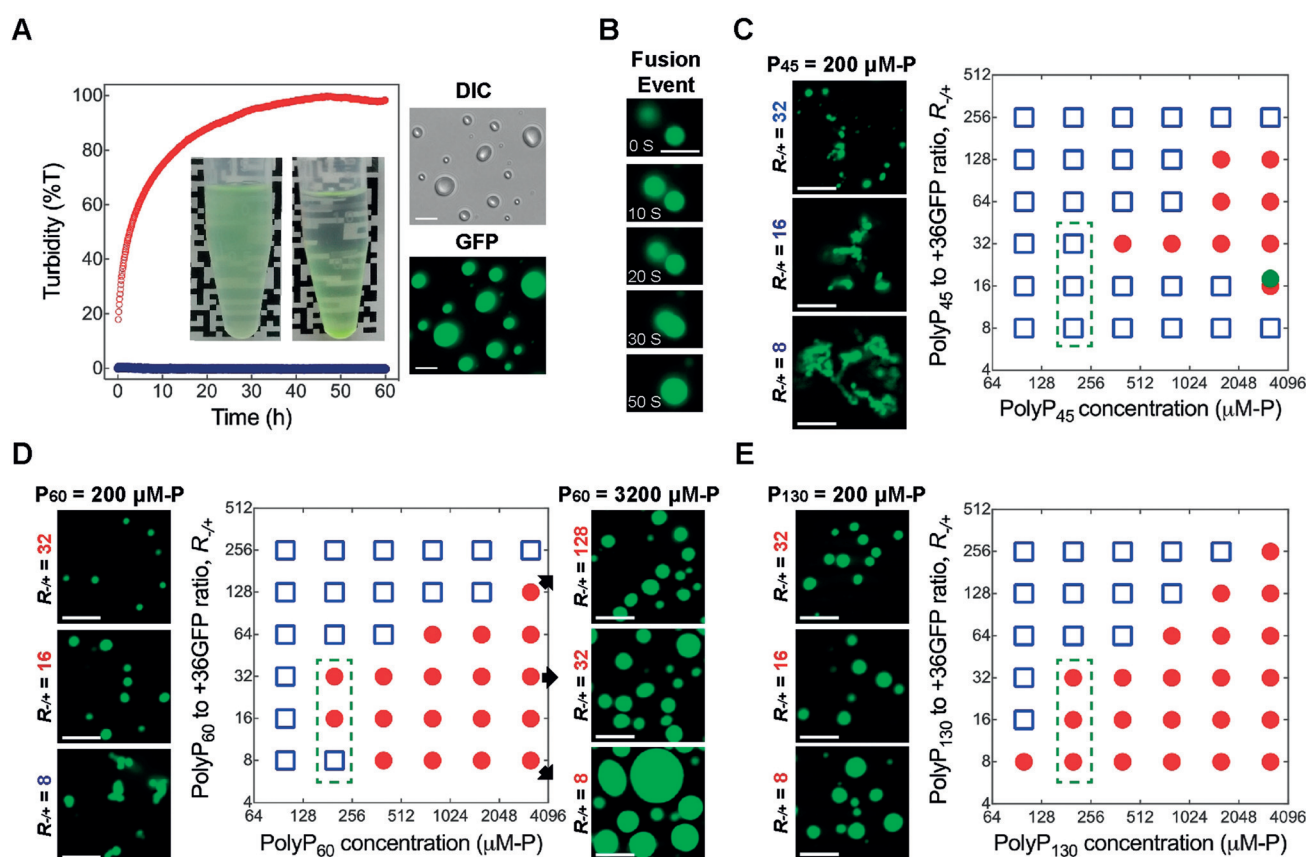


**Figure 3.** In vitro phase separation of +36GFP driven by polyP. A) Turbidity plot of +36GFP (blue circles) and +36GFP plus polyP (red circles) as a function of time. Insets are photographs of a turbid solution and gravity-induced coacervation, respectively. Right panel: images captured with the DIC module and GFP channel are given to show +36GFP droplet wetting on a glass surface. Scale bar, 10  $\mu\text{m}$ . The images are representative of all fields on the glass bottom of Petri dishes. B) Fusion of two +36GFP droplets. Time scale, seconds. Scale bar, 5  $\mu\text{m}$ . The images are representative of at least five fused droplets. C) Phase distribution of +36GFP driven by heterogeneous polyP<sub>45</sub>, with respect to polyP concentration and the net charge ratio of polyP to +36GFP,  $R_{+/+}$ . Solid red circles indicate polyP concentration for which spherical +36GFP droplets were observed, while empty blue squares represent no coacervate droplets were observed. The solid green circle corresponds to the given polyP concentration and  $R_{+/+}$ , under which condition bulk liquid turbidity was determined in (A) and the fusion event was captured in (B). D) Phase distribution of +36GFP driven by homogenous polyP<sub>60</sub>. Images shown on the right side correspond to the icons indicated by the black arrows on the plot, which were extracted to show the increased total droplet area as a function of decreasing  $R_{+/+}$ . Scale bar, 5  $\mu\text{m}$ . E) Phase distribution of +36GFP driven by homogenous polyP<sub>130</sub>. Scale bar, 5  $\mu\text{m}$ . The images shown in (C), (D), and (E) are representative of all fields on the glass bottom of Petri dishes. Images shown on the left side correspond to the icons that are indicated by the dashed green line on the phase plot, which were extracted to aid in the visualization of the phase boundary and for the comparison of polyP with different chain lengths. All the experiments were conducted independently at least three times.  $\mu\text{M}\cdot\text{P}$  = phosphate concentration.

polyP molecules is chain-length dependent—the longer the chain length, the more potent the driven force. Increasing the chain length of polyanions might increase the probability of the system crossing the critical point, which is a prerequisite for the occurrence of LLPS.<sup>[13]</sup>

Increasing evidence has shown that the intracellular environment in cells is organized into membraneless compartments, termed biomolecular condensates because they are formed by LLPS.<sup>[6c,14]</sup> Cells could further spatially and temporally organize their cytoplasm and nucleoplasm to fulfil specific physiological functions. Interestingly, a recent breakthrough by Knowles and Yan showed that LLPS is a crucial step prior to the nucleation of supramolecular nanofibrils with either amphiphilic amino acids or short peptides in vitro.<sup>[15]</sup> In this study, we show that the endogenous inorganic polyphosphate polyP can manipulate posi-

tively charged proteins to perform LLPS in cells. This LLPS mediated by polyP was related to intermolecular electrostatic interactions. When mixing polyP with +36GFP, complexes of oppositely charged polyions were formed to lower the net charge and drive phase separation via a process referred to as complex coacervation.<sup>[16]</sup> As a result, both polyP and +36GFP are recruited and highly concentrated in the polymer-rich droplets. It is worth mentioning that there are other interaction modes between polyP and its protein clients, as listed in Table 1.

PolyP is conserved from bacteria to mammalian cells where it is involved in vital physiological functions. Our results suggest that polyP induces the phase separation of positively charged proteins in the crowded cytoplasm where high concentrations of negatively charged nucleic acids (DNA and RNA) exist. A stronger binding ability of polyP, arising

**Table 1:** Protein clients of polyP and proposed interaction modes.<sup>[a]</sup>

Target Protein	Interaction Mode	Biological Process	Reference
Lon protease + 36GFP	Domain binding LLPS	Protein degradation; ageing n/a	Kornberg et al. <sup>[1a]</sup> This study
Luciferase	Electrostatic repulsion	Chemiluminescence; reporter	Jakob et al. <sup>[4a]</sup>
Citrate synthases	Electrostatic attraction	TCA cycle	Jakob et al. <sup>[4a]</sup>
CsgA	Electrostatic repulsion	Biofilm formation; pathogenic	Jakob et al. <sup>[4b]</sup>
Human Tau	Nucleation	Amyloidogenic procession	Jakob et al. <sup>[4b]</sup>
β <sub>2</sub> -microglobulin	Electrostatic repulsion (acid pH) Hofmeister effects (neutral pH)	Amyloidogenic procession	Goto et al. <sup>[5]</sup>

[a] n/a = not applicable.

from its increased charge density compared to nucleic acids, could account for this phenomenon. Our findings suggest a general approach to manipulate protein–protein interactions via inorganic polyP-mediated LLPS. Further studies on the polyP-induced intracellular “phase-separating network” are under way.

### Acknowledgements

We thank Dr. Toshikazu Shiba (Regenitiss, Japan) for kindly providing us with inorganic polyphosphates of different chain lengths. Financial support was provided by the National Science Foundation of China (21622103, 21571098, 21671099 and 91753121), and the Shenzhen Basic Research Program (JCYJ20180508182240106), Supported by the Fundamental Research Funds for the Central Universities (020514380139).

### Conflict of interest

The authors declare no conflict of interest.

**Keywords:** inorganic polyphosphate · phase separation · polyanions · polymers · protein–protein interactions

**How to cite:** *Angew. Chem. Int. Ed.* **2020**, *59*, 2679–2683  
*Angew. Chem.* **2020**, *132*, 2701–2705

- [1] a) A. Kuroda, K. Nomura, R. Ohtomo, J. Kato, T. Ikeda, N. Takiguchi, H. Ohtake, A. Kornberg, *Science* **2001**, *293*, 705–708; b) C. D. Fraley, M. H. Rashid, S. S. K. Lee, R. Gottschalk, J. Harrison, P. J. Wood, M. R. W. Brown, A. Kornberg, *Proc. Natl. Acad. Sci. USA* **2007**, *104*, 3526–3531; c) M. R. W. Brown, A. Kornberg, *Trends Biochem. Sci.* **2008**, *33*, 284–290.
- [2] R. Docampo, W. de Souza, K. Miranda, P. Rohloff, S. N. J. Moreno, *Nat. Rev. Microbiol.* **2005**, *3*, 251–261.
- [3] a) S. A. Smith, N. J. Mutch, D. Baskar, P. Rohloff, R. Docampo, J. H. Morrissey, *Proc. Natl. Acad. Sci. USA* **2006**, *103*, 903–908; b) X. H. Wang, S. F. Wang, F. He, E. Tolba, H. C. Schroder, B. Diehl-Seifert, W. E. G. Muller, *Adv. Eng. Mater.* **2016**, *18*, 1406–1417; c) A. Y. Abramov, C. Fraley, C. T. Diao, R. Winkfein, M. A. Colicos, M. R. Duchen, R. J. French, E. Pavlov, *Proc. Natl. Acad. Sci. USA* **2007**, *104*, 18091–18096.
- [4] a) M. J. Gray, W. Y. Wholey, N. O. Wagner, C. M. Cremers, A. Mueller-Schickert, N. T. Hock, A. G. Krieger, E. M. Smith, R. A. Bender, J. C. A. Bardwell, U. Jakob, *Mol. Cell* **2014**, *53*, 689–699; b) C. M. Cremers, D. Knoefler, S. Gates, N. Martin, J. U. Dahl, J. Lempart, L. H. Xie, M. R. Chapman, V. Galvan, D. R. Southworth, U. Jakob, *Mol. Cell* **2016**, *63*, 768–780.
- [5] C. M. Zhang, K. Yamaguchi, M. So, K. Sasahara, T. Ito, S. Yamamoto, I. Narita, J. Kardos, H. Naiki, Y. Goto, *Proc. Natl. Acad. Sci. USA* **2019**, *116*, 12833–12838.
- [6] a) S. Maharana, J. Wang, D. K. Papadopoulos, D. Richter, A. Pozniakovskiy, I. Poser, M. Bickle, S. Rizk, J. Guillen-Boixet, T. M. Franzmann, M. Jahnel, L. Marrone, Y. T. Chang, J. Sternecker, P. Tomancak, A. A. Hyman, S. Alberti, *Science* **2018**, *360*, 918–921; b) M. J. Du, Z. J. J. Chen, *Science* **2018**, *361*, 704–709; c) C. P. Brangwynne, C. R. Eckmann, D. S. Courson, A. Rybarska, C. Hoegel, J. Gharakhani, F. Julicher, A. A. Hyman, *Science* **2009**, *324*, 1729–1732.
- [7] a) P. L. Li, S. Banjade, H. C. Cheng, S. Kim, B. Chen, L. Guo, M. Llaguno, J. V. Hollingsworth, D. S. King, S. F. Banani, P. S. Russo, Q. X. Jiang, B. T. Nixon, M. K. Rosen, *Nature* **2012**, *483*, 336–U129; b) S. F. Banani, H. O. Lee, A. A. Hyman, M. K. Rosen, *Nat. Rev. Mol. Cell Biol.* **2017**, *18*, 285–298; c) N. Martin, L. F. Tian, D. Spencer, A. Coutable-Pennarun, J. L. R. Anderson, S. Mann, *Angew. Chem. Int. Ed.* **2019**, *58*, 14594–14598; *Angew. Chem.* **2019**, *131*, 14736–14740.
- [8] X. Wang, X. M. Wang, K. M. Hui, W. Wei, W. Zhang, A. J. Miao, L. Xiao, L. Y. Yang, *Environ. Sci. Technol.* **2018**, *52*, 214–222.
- [9] M. S. Lawrence, K. J. Phillips, D. R. Liu, *J. Am. Chem. Soc.* **2007**, *129*, 10110–10112.
- [10] D. Ault-Riche, C. D. Fraley, C. M. Tzeng, A. Kornberg, *J. Bacteriol.* **1998**, *180*, 1841–1847.
- [11] W. M. Aumiller, C. D. Keating, *Nat. Chem.* **2016**, *8*, 129–137.
- [12] H. Y. Zhang, S. Elbaum-Garfinkle, E. M. Langdon, N. Taylor, P. Occhipinti, A. A. Bridges, C. P. Brangwynne, A. S. Gladfelter, *Mol. Cell* **2015**, *60*, 220–230.
- [13] C. P. Brangwynne, P. Tompa, R. V. Pappu, *Nat. Phys.* **2015**, *11*, 899–904.
- [14] a) S. Saha, C. A. Weber, M. Nusch, O. Adame-Arana, C. Hoegel, M. Y. Hein, E. Osborne-Nishimura, J. Mahamid, M. Jahnel, L. Jawerth, A. Pozniakovski, C. R. Eckmann, F. Julicher, A. A. Hyman, *Cell* **2016**, *166*, 1572–1584; b) X. L. Su, J. A. Ditlev, E. F. Hui, W. M. Xing, S. Banjade, J. Okrut, D. S. King, J. Taunton, M. K. Rosen, R. D. Vale, *Science* **2016**, *352*, 595–599; c) H. B. Zhou, Z. H. Song, S. Zhong, L. Y. Zuo, Z. Qi, L. J. Qu, L. H. Lai, *Angew. Chem. Int. Ed.* **2019**, *58*, 4858–4862; *Angew. Chem.* **2019**, *131*, 4912–4916.
- [15] C. Yuan, A. Levin, W. Chen, R. Xing, Q. Zou, T. W. Herling, P. K. Challa, T. P. J. Knowles, X. Yan, *Angew. Chem. Int. Ed.* **2019**, *131*, 18284–18291.
- [16] A. Veis, *Adv. Colloid Interface Sci.* **2011**, *167*, 2–11.

Manuscript received: October 30, 2019

Accepted manuscript online: November 19, 2019

Version of record online: January 16, 2020